Research article

# Combination of silicene and boronene as a potential anode material for high-performance lithium-ion batteries: Insights from first principles

Hai-lin Ren [a,b], Yang Su [b], Shuai Zhao [b], Cheng-wei Li [b], Xiao-min Wang [a,*],
Bo-han Li [b], Bo-wen Zhang [a]

[a] *Xinjiang Key Laboratory of Novel Functional Materials Chemistry,College of Chemistry and Environmental Sciences, Kashi University, Kashi, 844000, China*
[b] *School of Materials and Metallurgy, University of Science and Technology Liaoning, Anshan, 114051, China*

A B S T R A C T

Material design is essential for the development and preparation of new materials. In this paper, a new two-dimensional heterostructure material (B@Si) consisting of boronene and silicene is designed and used as an anode material for lithium-ion batteries in order to improve the performance of lithium-ion batteries, and the structural properties, stability, electronic properties, and performance as an anode material for lithium-ion batteries are systematically investigated by first-principle calculations of the B@Si heterostructure. The results show that the B@Si heterostructure is energetically, thermodynamically and dynamically stable, and although the Dirac cone in the energy band structure of silicene disappears after the formation of the heterojunction, the overall electrical conductivity of the material improves considerably and the electron transport rate is faster. Due to the synergistic effect, Li has more stable adsorption sites and lower diffusion barriers than boronene and silicene in the B@Si heterostructure, higher theoretical specific capacity (1208 mAhg$^{-1}$), and stronger mechanical properties ($C_{11}$ = 296.6 N/m, $C_{22}$ = 142.8 N/m). The volume expansion in the fully lithiated state is also only 8 %. These advantages indicate that B@Si heterostructures are good potential anode materials for high-performance Li-ion batteries.

## 1. Introduction

Energy has been an issue that has plagued the entire world so far, and modern civilisation cannot develop without advanced energy systems. Since the commercialisation of lithium-ion batteries (LIBs) in 1991, they have been very relevant to people's lives [1]. In the lithium-ion battery has been developed for more than 30 years today, people's daily life in the use of mobile phones, laptop computers and new energy vehicles and other equipment on the energy demand is growing, so improve the energy density of lithium-ion batteries, cycle stability and other performance has been very urgent [2–4]. The performance of the anode material is particularly important in LIB, and the most widely commercialised anode material is graphite, which replaces the most traditional lithium metal. However, graphite has a low theoretical capacity of 372 mAhg$^{-1}$, which is no longer sufficient for the current demands of life. Si has

been considered the most promising alternative to graphite negative electrodes due to having the highest theoretical capacity ($\sim$4200 mAh g$^{-1}$). However, the higher theoretical capacity also means that Si will have a huge volume expansion in the fully lithiated state, which will lead to the microstructure rupture of the electrode material and the repeated regeneration of the solid electrolyte interface (SEI) during the repeated embedding/de-embedding of lithium ions, which will lead to the irreversible depletion of lithium ions, and will seriously affect the cycle life and charging/discharging performance of the batteries, and this has seriously impeded the commercialisation of Si applications [5]. In order to overcome these problems, many scholars have proposed various solutions, such as reducing the size of Si particles, core-shell structures, silicon nanotubes, C/Si composites, etc [6–8]. Sung et al. used ethylene as an inhibitor of Si crystal growth to slow down the growth of nucleated Si through Si-C bond formation, and ultimately synthesised Si particles achieving sub-nanometer size. The sub-nanometer-sized Si anode improved cycling stability (99.96 % Coulombic efficiency in 50 cycles) and 91 % capacity retention after 2875 cycles [9]. Xiao et al. constructed a nanoscale porous core-shell structure that exhibits a high diffusion rate and reversible inward volume expansion/contraction of lithium ions, with a reversible capacity of 1800 mAh g$^{-1}$ after 200 cycles at a current density of 180 mAg$^{-1}$ [10].

In addition to the alteration of Si in three-dimensional structures, researchers have gradually shifted their perspective to two-dimensional (2D) structures of silicon, which typically have higher surface area and lower Li diffusion barriers, making them a high-quality choice of anode materials for lithium-ion batteries [11]. Since 1994, when Takeda and Shiraish proposed silicene materials with graphene-like structures, it was only in recent years that it has been synthesised on the substrates of Ag(110), Ag(111), Ir (111) and ZrB$_2$ [12–14]. Although silicene is similar to graphene in that it is a single-layer 2D structure, it is a semiconductor with a very small bandgap and its surface is not as smooth as graphene's, which exhibits an overall flexural structure [15]. Although there are no relevant experiments to prove that silicene can be used as an anode material for lithium-ion batteries. However, Tritsaris et al. investigated the interaction of single-layer silicene (SL) and double-layer silicene (DL) with Li, as well as the Li storage properties, using density-functional theory (DFT) calculations. Theoretical results show that silicene is a very promising anode material for lithium-ion batteries, with much higher theoretical capacity than graphite, with SL and DL of 954 mAhg$^{-1}$ and 715 mAhg$^{-1}$, and a very small volume change ($\sim$13%–24 %) after complete lithium embedding [16]. The adsorption energy of Li on silicene is about 1.89 eV–2.2 eV, which is much larger than that on graphite (0.6 eV–1.3 eV). However, because of the flexural structure of silicene and the strong internal spin-orbit coupling effect, silicene is softer than graphene, and the in-plane stiffness is only 20 % of that of graphene, and the overall strength is lower, which also leads to the embedded lithium in silicene will undergo a large structural change, and in the natural world it is difficult to exist in the form of a monolayer, all to be dependent on the substrate [17,18]. Considering the existence of these problems, there is a need to select a suitable substrate for silicene to improve its properties.

Boronene, also a graphene-like 2D layered material. Since Oganov, Hersam et al. successfully synthesised it on the Ag surface (111) under vacuum conditions in 2015, numerous researchers have embarked on the study of boronene [19]. Boronene has a similar flexural structure to silicene and can also be used as an anode material for lithium-ion batteries, with not only good conductivity, but also low diffusion barriers, strong Li binding energy and a theoretical capacity of 620 mAhg$^{-1}$. Most importantly, boronene also has greater stiffness and hardness than graphene [20,21]. Considering these advantages, it is very intriguing to see how the heterojunction changes when formed with boronene and silicene. There are no reports of any heterojunction consisting of boronene and silicene.

In this work, this paper uses first principles to explore the structural changes, energetic stability, kinetic stability, thermodynamic stability, and electronic properties of boronene and silicene when they form a heterojunction. The adsorption and diffusion behaviour of Li on B@Si heterostructures and the lithium storage capacity were also systematically investigated.

## 2. Calculation method

All calculations in this paper are based on Density Functional Theory (DFT) and are done in the Castep module on the Materials Studio software [22]. Calculation of all ion-electron exchange energies using the generalised gradient approximation (GGA) and the Perdew-Burke-Ernzerhof (PBE) method with the introduction of an ultrasoft pseudopotential [23,24]. Description of remote van der Waals interactions during Li-ion adsorption using Grimme dispersion correction. In order to eliminate the periodic interactions in the z-direction, a vacuum layer of 15 Å was added. After convergence testing of the whole system (energy error less than 1 meV/atom), the plane-wave cut-off energy was set to 650 eV and Brillouin zone on 5 × 3 × 1 and 8 × 4 × 1 Monkhorst package grids for atomic relaxation and electronic structure calculations. At the same time, in order to ensure sufficient accuracy, the restriction was relaxed for all atoms during the atomic relaxation phase until the self-consistent field energy (SCF) variation was less than $1 \times 10^{-6}$ eV/atom, the total energy variation was less than $1 \times 10^{-5}$ eV/atom, the maximum stress between atoms was less than 0.03 eV/Å, and the maximum ionic step was less than 0.001 Å. The minimum diffusion barrier path for Li in heterogeneous structures is predicted using the LST/QST (Linear Synchronous Transit/Quadratic Synchronous Transit) method [25,26].

In order to predict the stability of the heterogeneous structure, it is calculated by the following equation [27],

$$E_{binding} = \frac{E_{B@Si} - aE_B - bE_{Si}}{a + b} \tag{1}$$

where EB@Si is the total energy of the heterostructure, E$_B$ and E$_{Si}$ denote the energies of individual B and Si atoms, respectively, and a, b denote the number of B and Si atoms in the heterostructure, respectively. The strength of the interactions between silicene and boronene in the B@Si heterostructure is evaluated by the following equation,

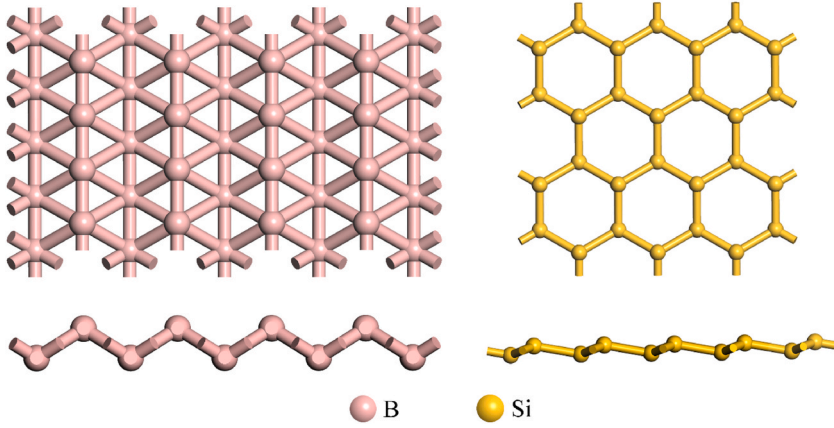$$E_{from} = E_{B@Si} - E_{Boronene} - E_{Silicene} \tag{2}$$

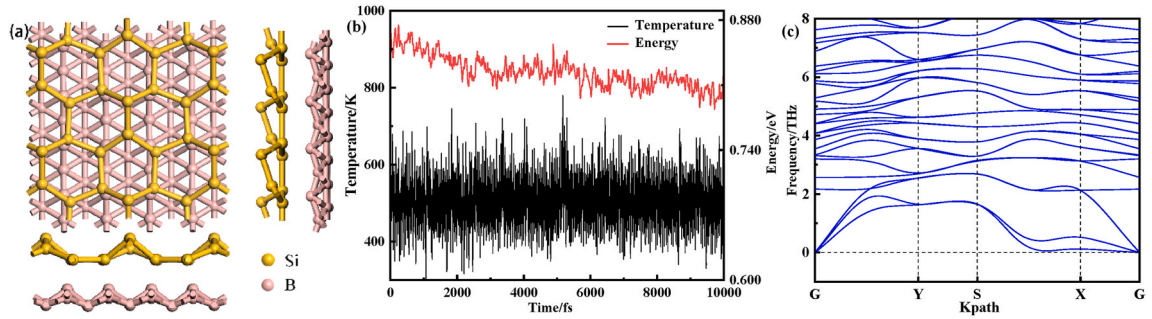**Fig. 1.** Structure schematics of boronene and silicene.



**Fig. 2.** (a) Schematic structure of B@Si (top and main view on the left and left view on the right) (b) Thermal stability test of B@Si heterostructures (c) Phonon scattering curves of B@Si heterostructures.

where $E_{Silicene}$ and $E_{Boronene}$ represent the energies of silicene and boronene prior to the formation of heterogeneous structures. The adsorption energy after adsorption of 'x' Li atoms on B@Si is defined as follows [28],

$$E_{ads} = \frac{E_{LixB@Si} - xE_{Li} - E_{B@Si}}{x} \tag{3}$$

where $E_{Li}$ represents the energy of isolated Li atoms and $E_{LixB@Si}$ represents the total energy of the heterostructure after adsorption of x Li atoms. The change in the open-circuit voltage of the structure during adsorption of Li is calculated by the following equation [29],

$$V_{ocp} = \frac{E_{LixB@Si} - x\mu_{Li} - E_{B@Si}}{xe} \tag{4}$$

where $\mu_{Li}$ denotes the chemical potential of bcc-Li. In order to evaluate the mechanical properties of the heterostructure of B@Si, Young's modulus and Poisson's ratio along the x and y directions were calculated using the following equations [30].

$$Y_X = \frac{C_{11}C_{22} - C_{12}^2}{C_{22}} \quad Y_Y = \frac{C_{11}C_{22} - C_{12}^2}{C_{11}} \tag{5}$$

$$\upsilon_X = \frac{C_{12}}{C_{22}} \quad \upsilon_Y = \frac{C_{12}}{C_{11}} \tag{6}$$

where $C_{11}$ and $C_{22}$ represent the stiffnesses for stretching in the x and y directions, and $C_{12}$ represents the stiffness for stretching in both x and y simultaneously.

## 3. Results and discussion

### 3.1. Structural characteristics of B@Si

As shown in Fig. 1, both silicene and boronene exhibit a flexural structure after full relaxation under GGA-PBE calculations, with a

**Table 1**
Elastic constants $C_{ij}$ (N/m), Young's modulus Y (N/m) and Poisson's ratio of pristine Silicene, Boronene and B@Si heterostructure.

|          | $C_{11}$ | $C_{22}$ | $C_{12}$ | $C_{44}$ | $Y_x$ | $Y_y$ | $\upsilon_x$ | $\upsilon_y$ |
|----------|----------|----------|----------|----------|-------|-------|--------------|--------------|
| Silicene | 79.2     | 79.2     | 25.1     | 24.6     | 71.2  | 71.2  | 0.31         | 0.31         |
| Boronene | 251.6    | 107.9    | 5.7      | 486.7    | 251.2 | 107.7 | 0.05         | 0.02         |
| B@Si     | 296.6    | 142.8    | 29.8     | 503.8    | 190.3 | 139.8 | 0.20         | 0.10         |
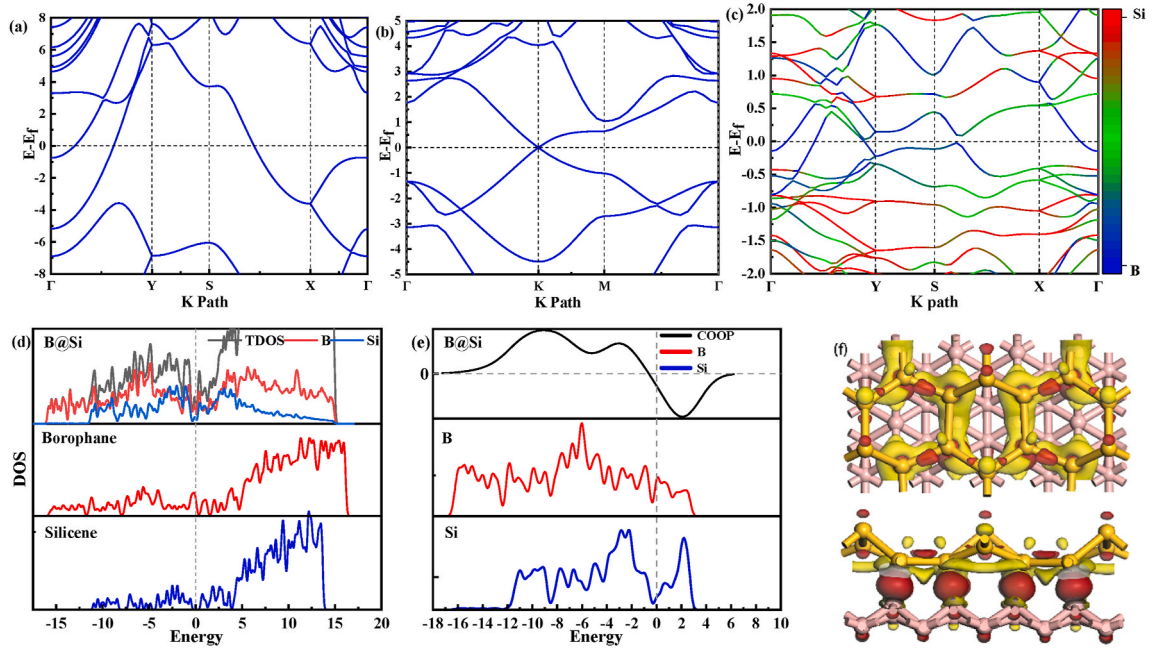


**Fig. 3.** (a, b) Electronic energy band structures of boronene and silicene, respectively (c) Projected energy band structure of B@Si (d) PDOS of B@Si (e) Crystal orbital overlap population of nearest B and Si atoms in B@Si (f) Differential charge density of B@Si (Red indicates gain of charge Yellow indicates loss of charge).

Si-Si bond length of 2.27 Å, a bond angle of 116.59°, a flexural height of 0.43 Å, and a lattice constant of 3.857 Å in silicene which is in agreement with other literature results [15,31–34]. There are two different B-B bonds in boronene, with a B-B bond length of 1.61 Å when two B atoms are in the same layer and 1.85 Å when two B atoms are in different layers. And there are also two bond angles in boronene, 51.57° and 64.21°. This calculation is in good agreement with experimental and other theoretical calculation papers [35, 36]. To reduce the lattice mismatch, the lattice of silicene was first converted from a rhombohedral crystal system to an orthorhombic one, and the heterojunctions were made with 4 × 4 boronene supercells (a = 6.46 Å, b = 11.34 Å) and 1 × 3 silicene supercells (a = 6.71 Å, b = 11.63 Å). The lattice constants of B@Si after full atomic relaxation are 6.46 Å and 11.44 Å, respectively, and the lattice mismatch is only 2.5 %, which indicates that the heterostructures established in this paper are fully rational.

The B@Si heterostructure is shown in Fig. 2a, where both boronene and silicene have undergone a large deformation after the formation of the heterojunction, both transforming from the original two-layer flexural structure to a three-layer flexural structure, with a final equilibrium layer spacing of 2.02 Å. The B@Si heterostructure is shown in Fig. 2a. $E_{binding} = -5.72$ eV and $E_{from} = -7.59$ eV for A calculated from Eq. (1)(2), which indicates that the B@Si heterostructure is very stable from the energy point of view and the formation process is a spontaneous reaction [37]. In addition the interfacial binding energy between silicene and boronene is about 102.62 meV/Å$^2$, which is much larger than the 20 meV/Å$^2$ for the vdW interaction, suggesting that there is an energy level hybridisation between them, which is connected by chemical bonding, which will be analysed in the subsequent discussion of this paper [38]. To further check the stability of the B@Si heterostructure, first-principles molecular dynamics (FPMD) and phonon scattering curve calculations (e.g., Fig. 2b–c) were performed in this paper. Fig. 2b shows the total energy of the heterogeneous structure as a function of time near the temperature of 500 K. It can be seen that the energy change is very small (less than 1 eV) no structural reorganisation occurs during the simulation time, which suggests that B@Si is thermodynamically very stable [39]. Moreover, no imaginary frequencies are found in the phonon scattering curves of Fig. 2c, indicating that it is also very stable from a dynamical point of view.

For a new material, its mechanical properties are essential. A good mechanical property reduces the volume expansion during lithium embedding/de-lithiation. Therefore this paper also explores the mechanical properties of pristine boronene, silicene and B@Si heterostructures. As shown in Table 1, all structures satisfy the Born-Huang criterion and are mechanically stable [40]. Silicenes are soft and isotropic. Boronene has highly anisotropic mechanical properties, and its in-plane elastic constants and Young's modulus are
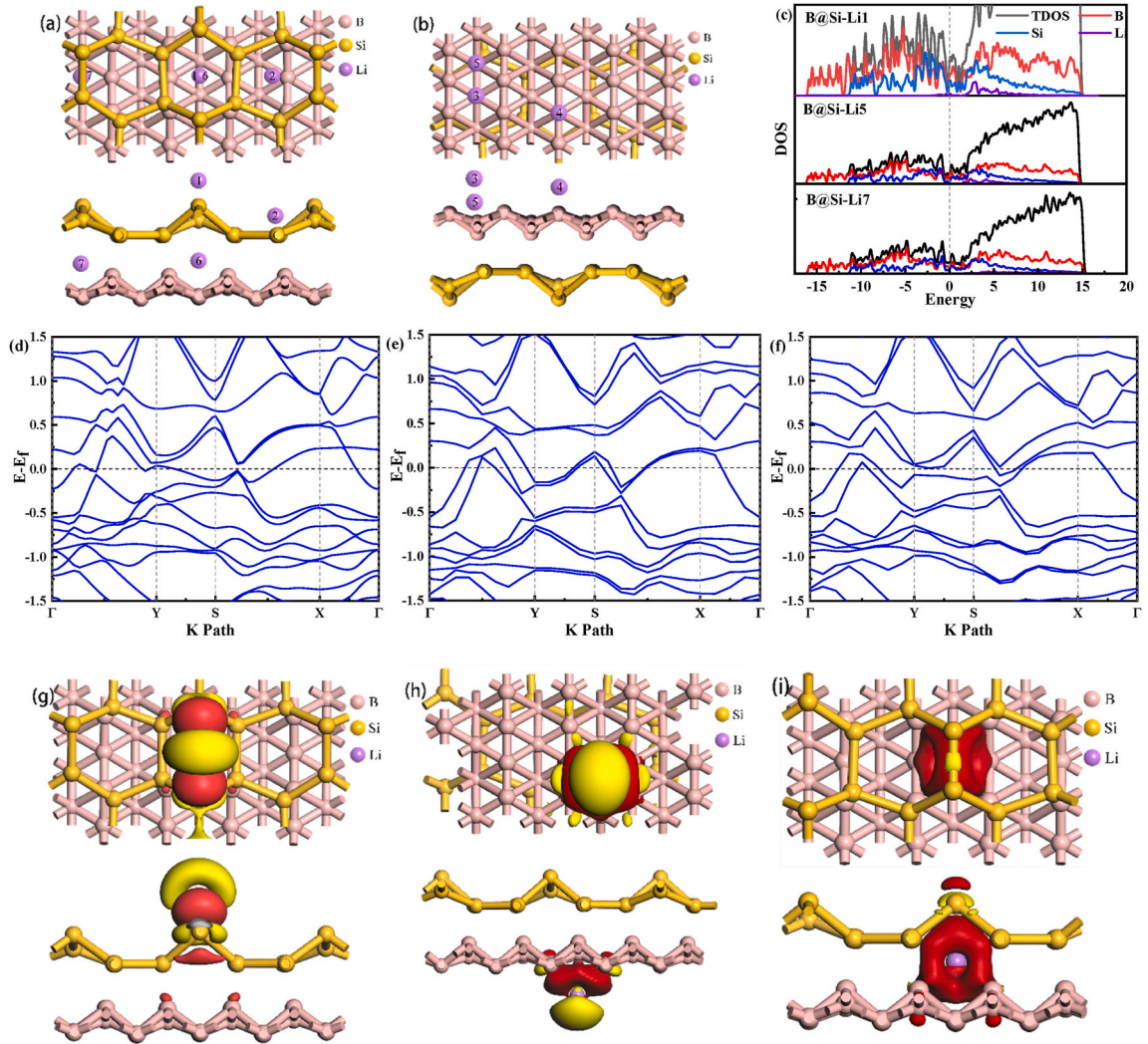
**Fig. 4.** (a, b) Schematic diagrams of the seven stable adsorption sites of Li (c) PDOS diagrams of B@Si-Li1, B@Si-Li4 and B@Si-Li7 (d–f) Electronic energy band structures of the three adsorption types (g–i) Differential charge density diagrams of the three adsorption types (Red indicates gain of charge Yellow indicates loss of charge).

much larger than those of silicene. Therefore, after forming a heterostructure with boronene as the substrate and silicene, B@Si maintains anisotropic mechanical properties and has higher in-plane elastic constants and Young's modulus than boronene and silicene. The enhanced mechanical properties help to avoid volume expansion of the electrodes, thus increasing the cycle life of the LIB.

### 3.2. Electronic properties of B@Si

The energy band structures of silicene, boronene and B@Si heterostructures are plotted in Fig. 3a–c. Due to the low flexural structure of silicene, an intrinsic Rashba SOC occurs, so that silicene can be seen to have a Dirac point with a bandgap of about 2 meV, which is typical of semiconductor structures [41–43]。 The conductivity of boronene exhibits a high degree of anisotropy, with no band gap arising when electrons pass through the Fermi energy levels in the ripple-free direction, exhibiting metallicity, but a large band gap occurs when electrons pass through in the ripple direction (Y-S, X-Γ). When they are stacked into a heterostructure, their energy band structure changes significantly, with some energy level hybridisation between boronene and silicene. Combining the projected energy bands in Fig. 3c and the projected density of states in Fig. 3d, it can be found that the energy bands near the Fermi energy level are mainly contributed by boronene only a very small amount is contributed by silicene, which leads to the disappearance of the Dirac cone of silicene. Moreover, the anisotropy of boronene is significantly improved, and the band gaps of the energy bands along the ripple direction (Y-S and X-Γ in the Brillouin zone) are significantly reduced or even disappeared [44]. An interaction between the sp hybridisation orbitals of Si and the sp hybridisation orbitals of B is also observed in the projected state density. Combined with the results of the analysis of the crystal orbital Hamiltonian layouts between the first layer of Si and the third layer of B in Fig. 3f, it

**Table 2**
Changes of each structure after Li adsorption.

|  | B@Si-Li1 | B@Si-Li2 | B@Si-Li3 | B@Si-Li4 | B@Si-Li5 | B@Si-Li6 | B@Si-Li7 | Silicene | Boronene |
|---|---|---|---|---|---|---|---|---|---|
| $-E_{ads}$ | 2.589 | 2.436 | 2.119 | 1.846 | 2.315 | 1.929 | 2.565 | 2.187 | 2.078 |
| d | 1.517 | 1.7093 | 2.356 | 2.099 | 2.495 | \ | \ | 1.865 | 2.746 |
| $\Delta h$ | 2.012 | 2.025 | 2.041 | 2.046 | 2.037 | 2.051 | 2.048 | \ | \ |

**Table 3**
Charge transfer for each structure (negative numbers indicate gain of electrons, positive numbers indicate loss of electrons).

|  | B@Si-Li1 | B@Si-Li5 | B@Si-Li7 | Silicene | Boronene | B@Si |
|---|---|---|---|---|---|---|
| $Q_{Li}$ | 0.778 | 1.561 | 1.614 | 1.078 | 1.326 | \ |
| $Q_{Si}$ | 0.552 | 1.333 | 0.761 | −1.078 |  | 1.533 |
| $Q_B$ | −1.330 | −2.894 | −2.375 | \ | −1.326 | −1.533 |

is found that bonding orbitals are formed by the sp hybridisation orbitals of Si and B in the valence band, whereas anti-bonding orbitals are produced in the conduction band [45,46]. According to Mulliken charge analysis, the layout number of the Si-B bond at this point is 0.76 and the bond length is 2.04 Å. This further suggests that a stable chemical bonding connection is formed between Si and B, and that this is what leads to the large structural changes of the silicene and boronene after the formation of the heterojunction. It can also be found in the differential charge density map of B@Si (in Fig. 3e) that charge transfer mainly exists in the two-phase interfacial region, with charge accumulation occurring in boronene charge depletion in silicene, and a total of 1.533 |e| being transferred from silicene to boronene.

*3.3. Li adsorption characteristics on B@Si*

Next this paper investigates the adsorption properties of B@Si heterostructure on Li. For this heterostructure, three very typical adsorption positions exist, the outer part of the silicene (Li/silicene/boronene), the middle of the B@Si heterostructure (silicene/Li/boronene) and the outer part of the boronene (silicene/boronene/Li). Seven major adsorption sites were observed after sufficient atomic relaxation (shown in Fig. 4). The adsorption energy ($-E_{ads}$), adsorption height (d), and layer spacing ($\Delta h$) after adsorption for each adsorption structure are shown in Table 2. Among these 7 adsorption configurations B@Si-Li1 and B@Si-Li2 belong to the first adsorption type, B@Si-Li3, B@Si-Li4 and B@Si-Li5 belong to the second adsorption type and B@Si-Li6 and B@Si-Li7 belong to the third adsorption type. The most stable adsorption positions of Li among these three adsorption types are B@Si-Li1, B@Si-Li4, and B@Si-Li7, and B@Si-Li1 has the shortest adsorption distance (1.517 Å) and the lowest adsorption energy (−2.589 eV), and its adsorption stability is much higher than that of boronene and silicene. The adsorption position of Li has a large effect on the layer spacing of the B@Si heterostructures, which swells to 2.037–2.051 Å when Li is in the middle of the heterostructure and on the outside of the boronene, and shortens to 2.012–2.025 Å when Li is on the outside of the silicene. Overall, due to the synergistic effect, the B@Si heterostructure has stronger Li adsorption properties than both pristine silicene and boronene, and this improved adsorption performance can effectively inhibit the formation of lithium dendrites during charging and discharging, and improve the electrochemical performance of the anode material [47]. And the magnitude of the adsorption ability of these three types of adsorption is in the order of Li/silicene/boronene > silicene/Li/boronene > silicene/boronene/Li, which suggests that in the lithium embedding process, Li will occupy the outside of silicene first, then the middle of the B@Si heterostructure and finally the outside of boronene.

In order to further understand the interaction between Li and B@Si heterostructures, Mulliken charge analysis was done for the three most stable adsorption types in this paper and the results are shown in Table 3. It can be found that when Li is located on both sides of the heterojunction, the vast majority of the charge is transferred to the neighbouring boronene/silicene, with only a very small portion transferred to the more distant side. When Li is located in the middle of the heterojunction, it transfers charge to both sides at the same time, and the charge transferred to boronene (0.842e) is slightly larger than the charge transferred to silicene (0.772e). This phenomenon arises mainly due to the differences in bonding between Li and B and Si atoms, which will be discussed in detail in the next step. These results indicate that there is a significant charge transfer between Li and B@Si heterostructures and that the interaction is ionic. In addition, the data in Table 3 also show that the charge transfer between Li and boronene is always much higher than that between Li and silicene, and in order to further understand this phenomenon this paper also calculates the partial density of states (PDOS), the energy band structure, and the differential charge density of these three structures (shown in Fig. 4). The energy band structures of B@Si-Li1, B@Si-Li5 and B@Si-Li7 all show slight changes compared to B@Si, suggesting that the adsorption of Li on the heterostructure of B@Si is not purely physisorption. Surprisingly, the presence of the Dirac cone is again observed in the energy band structure of B@Si-Li5, although by this time the Dirac cone is already located in the valence band. This phenomenon may be due to the fact that Li weakens the effect of boronene on silicene after transferring charge to boronene, which is also consistent with previous analyses that both types of adsorption lead to an increase in the interlayer spacing of the B@Si heterostructure. The PDOS in all three structures exhibit the same metallicity as the pristine B@Si heterostructure and all have a higher density of states at the Fermi energy level than the pristine, suggesting that their conductivity improves upon lithium adsorption. Strong hybridisation effects between Li and B atoms are also observed near the Fermi energy levels of the B@Si-Li5 and B@Si-Li7 structures, and strong ionic Li-B bonds are produced when Li adsorbs on boronene according to Zhang et al. [35]. According to the Mulliken chemical bond layout analysis, the sp
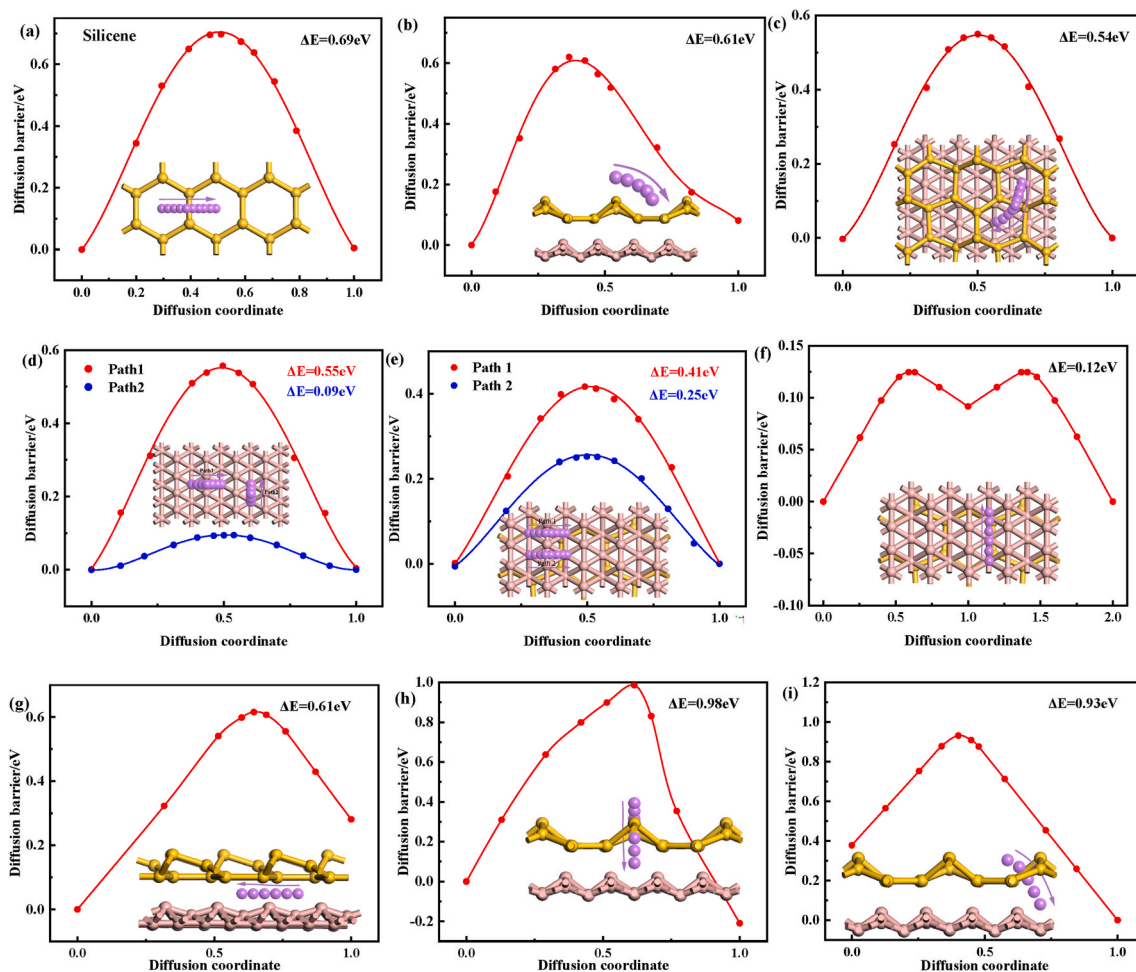
**Fig. 5.** (a) Diffusion energy barriers of Li on silicene (b) Diffusion energy barriers of Li from B@Si-Li1 to B@Si-Li2 (c) Diffusion of Li between two neighbouring B@Si-Li2 (d) Diffusion energy barriers of Li on boronene for two paths (e, f) Diffusion energy barriers of Li on boronene for three paths (g) Diffusion barriers of Li in the middle of a heterostructure (h, i) Li diffusion energy barriers from the first layer to the second layer.

hybridisation orbitals of Li and Si in the B@Si-Li1 structure will form strong covalent bonds, and the layout number of Li-Si bonds can reach 0.24, which indicates that the bonding between Li and boron alkene still belongs to the alloying reaction as in the case of conventional silicon anode. Finally, in conjunction with the charge density difference plots of Fig. 4g–i, it is found that charge depletion occurs in the vicinity of Li in all three structures, and in the B@Si-Li1 structure there will be a partial charge transfer to the middle of the B@Si heterostructure, which strengthens the connection between boronene and silicene. In the B@Si-Li5 and B@Si-Li7 structures there will be most of the electrons transferred to the boronene, which, together with their elevated Fermi energy levels (from −0.21 eV in the original B@Si heterostructures to 0.24 eV and −0.18 eV), leads to the fact that more electrons will enter into the antibonding orbitals, which will weaken the connection between the B-B bonds, which is shown in the differential charge density diagrams as the B-B bonds with charge depletion between them. This may be why Li has the largest charge transfer with boronene, but the stability of adsorbed Li is lower than Li adsorbed on silicene.

### 3.4. Diffusion behaviour of Li on B@Si heterostructures

It is well known that the rate charge/discharge performance of Li-ion batteries is highly dependent on the diffusion rate of Li on the electrode material [48,49]. Therefore, the study of Li diffusion on the surface of heterogeneous structures is of great importance. As a comparison, the diffusion energy barriers of Li on pristine silicene and boronene were similarly calculated in this paper, as shown in Fig. 5a–d. The diffusion energy barrier between neighbouring silicon six-membered rings along the surface of Li silicene is 0.69 eV. The diffusion paths on the surface of Li boronene consist of two main types, the first one is along the ripple direction (0.55 eV) and the second one is along the non-ripple direction (0.09 eV). Due to the complexity of the B@Si heterostructure, the diffusion of Li is divided into four parts in this paper, which are Li outside the silicene, outside the boronene, in the middle of the silicene and boronene, and Li transitioning in these three structures. The first is diffusion in the lithium/silicene/boronene structure, where Li has two stable
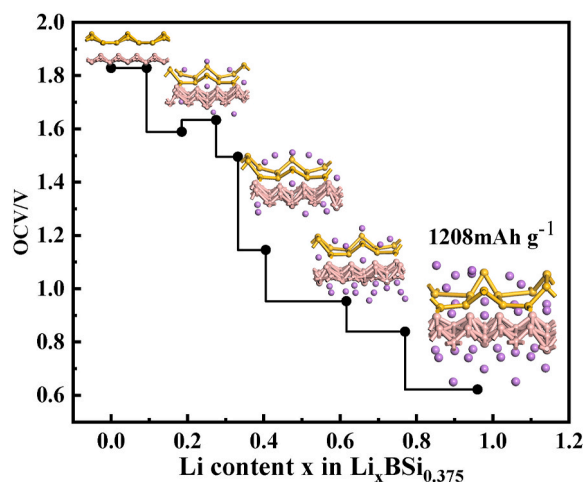
**Fig. 6.** Open circuit voltage (OCV) versus the amount of adsorbed Li for B@Si heterostructures.

adsorption sites (B@Si-Li1 and B@Si-Li2). In this paper, two types of diffusion are considered, the first being Li diffusion between B@Si-Li1 and B@Si-Li2, corresponding to a diffusion energy barrier of 0.61 eV. The second is the diffusion of Li between two neighbouring B@Si-Li2, corresponding to a diffusion energy barrier of 0.54 eV, which is calculated as shown in Fig. 5b-c.Similarly in silicene/boronene/Li there are three stable adsorption sites for Li (B@Si-Li3 and B@Si-Li4 and B@Si-Li5) and three diffusion pathways exist. The first is diffusion along the corrugation direction at the B@Si-Li3 position, the second is diffusion along the corrugation direction at B@Si-Li5, and the third is diffusion along the non-corrugation direction. As shown in Fig. 5e-f, it can be found that the diffusion energy barriers of Li along the corrugation direction are all reduced to different degrees, but the diffusion energy barriers in the non-corrugation direction become larger. This is mainly due to the fact that some of the B atoms form covalent bonds with the Si atoms, resulting in the B atoms no longer being in the same plane on the diffusion path. As shown in Fig. 5g, for the silicene/Li/-boronene structure, Li has two stable adsorption sites (B@Si-Li6 and B@Si-Li7), but there exists a strong interaction between B and Si in the middle of the heterojunction, and in this paper, we only found that Li in B@Si-Li7 diffuses along the non-corrugated direction of boronene, and it has a higher diffusion energy barrier (0.61 eV), while Li in B@Si-Li6 cannot achieve diffusion in the middle of the heterojunction, and can only pass through the six-membered ring of Si to form a Li/silicene/boronene structure, and then diffuse in the surface layer of silicene and then pass through the six-membered ring of Si into the middle of the heterojunction. Finally, there is the conversion of Li in these three structures, where Li can only enter the middle of the heterostructure from the six-membered ring of Si due to the very small gap between B-B in boronene. As shown in Fig. 5h-i for Li diffusion from B@Si-Li1 and B@Si-Li2 to B@Si-Li6, both of this diffusion have high diffusion barriers of 0.98 eV and 0.93 eV, respectively. Overall, although Li diffusion in the middle of the heterogeneous structure has a high energy barrier, the diffusion rate on both sides is greatly enhanced compared to the original structure.

The most critical parameter of whether a material can be used as an anode for lithium-ion batteries is the lithium storage capacity. According to the previous calculations, Li will be inserted layer by layer when B@Si is embedded with lithium, preferentially occupying the outer side of silicene then the middle of the heterostructure through the Si six-membered ring and finally the outer side of boronene, and the heterostructure will be slightly deformed by inserting Li additionally after all the stable adsorption sites have been occupied by Li. The variation of the average open-circuit voltage with specific capacity and the heterostructure from an unlithiated state to a fully lithiated state for $Li_xBSi0.375$ is given in Fig. 6, when Li is inserted in the first layer ($0 \leq x \leq 0.09$), the average voltage is predicted to be 1.828 V. As Li continues to be inserted ($0.09 \leq x \leq 0.185$), an extremely rapid decrease in voltage is observed, followed by a slight recovery of the open-circuit voltage when $0.185 \leq x \leq 0.275$. And the adsorption energy at this time also showed an increase in the phenomenon, which is mainly due to the fact that Li began to occupy the second and third layers, and the change in the structure of the material began to become smaller stability gradually increased. With the further embedding of Li, both the open-circuit voltage and the adsorption energy continue to decrease until $0.77 \leq x \leq 0.96$, when the open-circuit voltage reaches 0.62 V. At this time, the capacity reaches 1208 mAhg$^{-1}$, which is much higher than that of monolayers of boronene with 620 mAhg$^{-1}$ and silicene with 954 mAhg$^{-1}$. This indicates that the construction of heterostructure can substantially improve the lithium storage performance of the material. The lattice constants of B@Si in the fully lithium-embedded state become a = 6.76 Å and b = 11.81 Å. The final volume expansion is about 8 %, which is lower than that of the pristine silicene. This further indicates that using boronene as a substrate for silicene can effectively improve the mechanical properties.

## 4. Conclusions

(1) In this paper, a novel two-dimensional heterojunction structure is designed, and it is proved that this new structure is energetically, thermodynamically and dynamically stable by DFT, FPMD and phonon scattering curve calculations.

(2) Calculations of the electronic structure of the B@Si heterostructure show that boronene and silicene are connected by covalent bonds, electrons are transferred from silicene to boronene, and the overall electrical conductivity is increased after the formation of the heterojunction.

(3) Due to the synergistic effect, Li has more stable adsorption sites on the B@Si heterostructure, and lower diffusion energy barriers, which leads to the system will have better rate charge/discharge performance, lower volume expansion and higher theoretical specific capacity during charging and discharging.

## CRediT authorship contribution statement

**Hai-lin Ren:** Data curation, Investigation, Supervision, Writing – original draft, Writing – review & editing. **Yang Su:** Investigation, Validation. **Shuai Zhao:** Project administration, Software. **Cheng-wei Li:** Supervision, Validation. **Xiao-min Wang:** Methodology, Resources. **Bo-han Li:** Investigation, Software. **Bo-wen Zhang:** Formal analysis, Investigation.

## Declaration of competing interest

All authors declare no conflict of interest in this manuscript.

## Acknowledgment

## References

[1] S.M. Abu, M. Hannan, M.S.H. Lipu, M. Mannan, P. Ker, M.J. Hossain, T. Mahlia, State of the art of lithium-ion battery material potentials: an analytical evaluations, issues and future research directions, J. Clean. Prod. 394 (2023) 136246, https://doi.org/10.1016/j.jclepro.2023.136246.

[2] Q. Wang, Z. Liu, H. Feng, R. Jin, S. Zhang, S. Gao, Engineering Bi₂S₃/BiOI p-n heterojunction to sensitize TiO₂ nanotube arrays photoelectrodes for highly efficient solar cells and photocatalysts, Ceram. Int. 45 (2019) 3995–4002, https://doi.org/10.1016/j.ceramint.2018.11.075.

[3] C.P. Grey, D.S. Hall, Prospects for lithium-ion batteries and beyond—a 2030 vision, Nat. Commun. 11 (2020) 6279, https://doi.org/10.1038/s41467-020-19991-4.

[4] J. Xu, X. Cai, S. Cai, Y. Shao, C. Hu, S. Lu, S. Ding, High-energy lithium-ion batteries: recent progress and a promising future in applications, Energy Environ. Mater. 6 (2023) 12450, https://doi.org/10.1002/eem2.12450.

[5] T. Chen, J. Wu, Q. Zhang, X. Su, Recent advancement of SiOₓ based anodes for lithium-ion batteries, J. Power Sources 363 (2017) 126–144, https://doi.org/10.1016/j.jpowsour.2017.07.073.

[6] Y. Zhang, X. Qin, Y. Liu, C. Lei, T. Wei, Z. Guo, Double-shell-structured Si@Al₂O₃@C nanoparticles as high-performance anode materials for lithium-ion batteries, J. Alloys Compd. 923 (2022) 166428, https://doi.org/10.1016/j.jallcom.2022.166428.

[7] Q. Xu, J. Sun, Z. Yu, Y. Yin, S. Xin, S. Yu, Y. Guo, SiOₓ encapsulated in graphene bubble film: an ultrastable Li-ion battery anode, Adv. Mater. 30 (2018) 1707430, https://doi.org/10.1002/adma.201707430.

[8] X. Guo, Z. Yang, W. Wang, Y. Zhang, N. Yu, C. Lu, Silicon/carbon nanotubes anode for lithium-ion batteries: synthesis, interface and electrochemical performance, Surface. Interfac. 48 (2024) 104223, https://doi.org/10.1016/j.surfin.2024.104223.

[9] J. Sung, N. Kim, J. Ma, J.H. Lee, S.H. Joo, T. Lee, S. Chae, M. Yoon, Y. Lee, J. Hwang, S.K. Kwak, J. Cho, Subnano-sized silicon anode via crystal growth inhibition mechanism and its application in a prototype battery pack, Nat. Energy 6 (2021) 1164–1175, https://doi.org/10.1038/s41560-021-00945-z.

[10] Q. Xiao, M. Gu, H. Yang, B. Li, C. Zhang, Y. Liu, F. Liu, F. Dai, L. Yang, Z. Liu, X. Xiao, G. Liu, P. Zhao, S. Zhang, C. Wang, Y. Lu, M. Cai, Inward lithium-ion breathing of hierarchically porous silicon anodes, Nat. Commun. 6 (2015) 8844, https://doi.org/10.1038/ncomms9844.

[11] S. Das, S.U.D. Shamim, M.K. Hossain, F. Ahmed, M.A. Hossain, M.O. Rahman, A novel silicon-doped 2D Ti₂C MXene monolayer as high capacity stable anode material for lithium ion batteries: insight from density functional theory study, Appl. Surf. Sci. 600 (2022) 154173, https://doi.org/10.1016/j.apsusc.2022.154173.

[12] K. Takeda, K. Shiraishi, Theoretical possibility of stage corrugation in Si and Ge analogs of graphite, Phys. Rev. B 50 (1994) 14916–14922, https://doi.org/10.1103/PhysRevB.50.14916.

[13] B. Aufray, A. Kara, S. Vizzini, H. Oughaddou, C. Leandri, B. Ealet, G. Le Lay, Graphene-like silicon nanoribbons on Ag (110): A possible formation of silicene, Appl. Phys. Lett. 96 (2010) 183102, https://doi.org/10.1063/1.3419932.

[14] L. Meng, Y. Wang, L. Zhang, S. Du, R. Wu, L. Li, Y. Zhang, G. Li, H. Zhou, W.A. Hofer, H. Gao, Buckled silicene formation on Ir (111), Nano Lett. 13 (2013) 685–690, https://doi.org/10.1021/nl304347w.

[15] H. Shu, X. Liu, Interfacial electronic characteristics and tunable contact types in novel silicene/Janus Ga₂STe heterobilayers, Surface. Interfac. 35 (2022) 102451, https://doi.org/10.1016/j.surfin.2022.102451.

[16] G.A. Tritsaris, E. Kaxiras, S. Meng, E. Wang, Adsorption and diffusion of lithium on layered silicon for Li-ion storage, Nano Lett. 13 (2013) 2258–2263, https://doi.org/10.1021/nl400830u.

[17] Q. Peng, X. Wen, S. De, Mechanical stabilities of silicene, RSC Adv. 3 (2013) 13772–13781, https://doi.org/10.1039/C3RA41347K.

[18] M.E. Dávila, G.L. Lay, Silicene: genesis, remarkable discoveries, and legacy, Mater, Today Adv. 16 (2022) 100312, https://doi.org/10.1016/j.mtadv.2022.100312.

[19] A.J. Mannix, X. Zhou, B. Kiraly, J.D. Wood, D. Alducin, B.D. Myers, X. Liu, B.L. Fisher, U. Santiago, J.R. Guest, M.J. Yacaman, A. Ponce, A.R. Oganov, M. C. Hersam, N.P. Guisinger, Synthesis of borophenes : anisotropic , two-dimensional boron polymorphs, Science 350 (2015) 1513–1516, https://doi.org/10.1126/science.aad1080.

[20] M. Makaremi, B. Mortazavi, C.V. Singh, 2D Hydrogenated graphene-like borophene as a high capacity anode material for improved Li/Na ion batteries: a first principles study, Mater. Today Energy 8 (2018) 22–28, https://doi.org/10.1016/j.mtener.2018.02.003.

[21] S. Karimzadeh, B. Safaei, T. Jen, Investigation on electrochemical performance of striped ,β12 and χ3 Borophene as anode materials for lithium-ion batteries, J. Mol. Graph. Model. 120 (2023) 108423, https://doi.org/10.1016/j.jmgm.2023.108423.

[22] S.J. Clark, M.D. Segall, C.J. Pickard, P.J. Hasnip, M.I.J. Probert, K. Refson, M.C. Payne, First principles methods using CASTEP, Z. Krist.-Cryst. Mater. 220 (2005) 567–570, https://doi.org/10.1524/zkri.220.5.567.65075.

[23] J.P. Perdew, K. Burke, M. Ernzerhof, Generalized gradient approximation made simple, Phys. Rev. Lett. 77 (1998) 3865–3868, https://doi.org/10.1103/PhysRevLett.77.3865.

[24] J.P. Perdew, J.A. Chevary, S.H. Vosko, K.A. Jackson, M.R. Pederson, D.J. Singh, C. Fiolhais, Atoms, molecules, solids, and surfaces: applications of the generalized gradient approximation for exchange and correlation, Phys. Rev. B 48 (1992) 4978, https://doi.org/10.1103/PhysRevB.46.6671.

[25] T.A. Halgren, W.N. Lipscomb, The synchronous-transit method for determining reaction pathways and locating molecular transition states, Chem. Phys. Lett. 49 (1977) 225–232, https://doi.org/10.1016/0009-2614(77)80574-5.

[26] N. Govind, M. Petersen, G. Fitzgerald, D. King-Smith, J. Andzelm, A generalized synchronous transit method for transition state location, Comput. Mater. Sci. 28 (2003) 250–258, https://doi.org/10.1016/S0927-0256(03)00111-3.

[27] T.M. Dieb, Z. Hou, K. Tsuda, Structure prediction of boron-doped graphene by machine learning, J. Chem. Phys. 148 (2018) 241716, https://doi.org/10.1063/1.5018065.

[28] S.U.D. Shamim, D. Roy, S. Alam, A.A. Piya, M.S. Rahman, M.K. Hossain, F. Ahmed, Doubly doped graphene as gas sensing materials for oxygen-containing gas molecules: a first-principles investigation, Appl. Surf. Sci. 596 (2022) 153603, https://doi.org/10.1016/j.apsusc.2022.153603.

[29] R. Li, P. Zhao, X. Qin, H. Li, D.E. Jiang, First-principles study of heterostructures of MXene and nitrogen-doped graphene as anode materials for Li-ion batteries, Surface. Interfac. 21 (2020) 100788, https://doi.org/10.1016/j.surfin.2020.100788.

[30] B. Mortazavi, F. Shojaei, X. Zhuang, Ultrahigh stiffness and anisotropic Dirac cones in BeN$_4$ and MgN$_4$ monolayers: a first-principles study, Mater. Today Nano 15 (2021) 100125, https://doi.org/10.1016/j.mtnano.2021.100125.

[31] M.J. Momeni, M. Mousavi-Khoshdel, E. Targholi, First-principles investigation of adsorption and diffusion of Li on doped silicenes: prospective materials for lithium-ion batteries, Mater. Chem. Phys. 192 (2017) 125–130, https://doi.org/10.1016/j.matchemphys.2017.01.082.

[32] H. Shu, Tensile strain effects on electronic and optical properties of functionalized diamondene-like Si$_4$, J. Mater. Sci. 56 (2021) 5684–5696, https://doi.org/10.1007/s10853-020-05622-2.

[33] J.A. Yan, S.P. Gao, R. Stein, G. Coard, Tuning the electronic structure of silicene and germanene by biaxial strain and electric field, Phys. Rev. B 91 (2015) 245403.1–245403.7, https://doi.org/10.1103/PhysRevB.91.245403.

[34] H. Shu, Y. Tong, J. Guo, Novel electronic and optical properties of ultrathin silicene/arsenene heterostructures and electric field effects, Phys. Chem. Chem. Phys. 19 (2017) 10644–10650, https://doi.org/10.1039/C7CP00695K.

[35] Y. Zhang, Z. Wu, P. Gao, S. Zhang, Y. Wen, Could borophene Be used as a promising anode material for high-performance lithium ion battery? ACS Appl. Mater. Interfaces 8 (2016) 22175–22181, https://doi.org/10.1021/acsami.6b05747.

[36] H. Chen, W. Zhang, X. Tang, Y. Ding, J. Yin, J. Jiang, P. Zhang, H. Jin, First principles study of P-doped borophene as anode materials for lithium ion batteries, Appl. Surf. Sci. 427 (2018) 198–205, https://doi.org/10.1016/j.apsusc.2017.08.178.

[37] H.R. Jiang, Z. Lu, M.C. Wu, F. Ciucci, T.S. Zhao, Borophene : a promising anode material offering high specific capacity and high rate capability for lithium-ion batteries, Nano Energy 23 (2016) 97–104, https://doi.org/10.1016/j.nanoen.2016.03.013.

[38] A. Castellanos-Gomez, X. Duan, Z. Fei, H.R. Gutierrez, Y. Huang, X. Huang, J. Quereda, Q. Qian, E. Sutter, P. Sutter, Van der Waals heterostructures, Nat. Rev. Methods Primers. 2 (2022) 58, https://doi.org/10.1038/s43586-022-00139-1.

[39] H. Lin, R. Jin, S. Zhu, Y. Huang, C$_3$N/blue phosphorene heterostructure as a high rate-capacity and stable anode material for lithium ion batteries: insight from first principles calculations, Appl. Surf. Sci. 505 (2020), https://doi.org/10.1016/j.apsusc.2019.144518.

[40] J.Q. Liu, Q. Gao, Z.P. Hu, HSH-carbon: a novel sp2–sp3 carbon allotrope with an ultrawide energy gap, Front. Physiol. 17 (2022) 1–6, https://doi.org/10.1007/s11467-022-1187-9.

[41] C. Liu, H. Jiang, Y. Yao, Low-energy effective Hamiltonian involving spin-orbit coupling in silicene and two-dimensional germanium and tin, Phys. Rev. B 84 (2011), https://doi.org/10.1103/PhysRevB.84.195430.

[42] Y. Guo, C. Ma, S. Gong, C. Zhao, T. Wang, X. Dong, S. Jiao, S. Ma, G. Xu, Y. An, J. Chen, Magnetic nanodevices and spin-transport properties of a two-dimensional Cr S Cl monolayer, Phys. Rev. Appl. 19 (2023) 054013, https://doi.org/10.1103/PhysRevApplied.19.054013.

[43] J. Liao, H. Wang, Y. Wu, Y. Li, K. Wang, C. Ma, S. Gong, T. Wang, X. Dong, Z. Jiao, Y. An, Y. Gao, Electronic transport properties and nanodevice designs for monolayer MoSi$_2$P$_4$, Phys. Rev. Appl. 18 (2022) 034033, https://doi.org/10.1103/PhysRevApplied.18.034033.

[44] H.H. Cocoletzi, J.E.C. Aguila, DFT studies on the Al , B , and P doping of silicene, Superlattice. Microst. 114 (2018) 242–250, https://doi.org/10.1016/j.spmi.2017.12.040.

[45] X. Liu, Y. Jiao, Y. Zheng, M. Jaroniec, S. Qiao, Building up a picture of the electrocatalytic nitrogen reduction activity of transition metal single-atom catalysts, J. Am. Chem. Soc. 141 (2019) 9664–9672, https://doi.org/10.1021/jacs.9b03811.

[46] Y. An, Y. Hou, K. Wang, S. Gong, R. Wu, Multifunctional lateral transition-metal disulfides heterojunctions, Adv. Funct. Mater. 30 (2020) 2002939, https://doi.org/10.1002/adfm.202002939.

[47] D. Wang, Y. Liu, X. Meng, Y. Wei, Y. Zhao, Q. Pang, G. Chen, Two-dimensional VS$_2$ monolayers as potential anode materials for lithium-ion batteries and beyond: first-principles calculations, J. Mater. Chem. A 5 (2017) 21370–21377, https://doi.org/10.1039/c7ta06944h.

[48] Le Shi, T. Zhao, Recent advances in inorganic 2D materials and their applications in lithium and sodium batteries, J. Mater. Chem. A 5 (2017) 3735–3758, https://doi.org/10.1039/C6TA09831B.

[49] J. Zhang, L. Xu, C. Yang, X. Zhang, L. Ma, M. Zhang, J. Lu, Two-dimensional single-layer PC$_6$ as promising anode materials for Li-ion batteries: the first-principles calculations study, Appl. Surf. Sci. 510 (2020) 145493, https://doi.org/10.1016/j.apsusc.2020.145493.